Acta Pharmaceutica Sinica B 2019;9(5):1008–1020

Chinese Pharmaceutical Association
Institute of Materia Medica, Chinese Academy of Medical Sciences

Acta Pharmaceutica Sinica B

www.elsevier.com/locate/apsb
www.sciencedirect.com

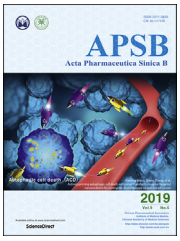

ORIGINAL ARTICLE

Upregulation of miR-489-3p and miR-630 inhibits oxaliplatin uptake in renal cell carcinoma by targeting OCT2

Lu Chen[a], Le Chen[a], Zhiyuan Qin[a], Jinxiu Lei[a], Sheng Ye[b], Kui Zeng[a], Hua Wang[c], Meidan Ying[a], Jianqing Gao[a], Su Zeng[a], Lushan Yu[a,*]

[a]*Institute of Drug Metabolism and Pharmaceutical Analysis, Zhejiang Province Key Laboratory of Anti-Cancer Drug Research, College of Pharmaceutical Sciences, Zhejiang University, Hangzhou 310058, China*
[b]*Paediatric Intensive Care Unit, the Children's Hospital, Zhejiang University School of Medicine, Hangzhou 310003, China*
[c]*Department of Urology, Cancer Hospital of Zhejiang Province, Hangzhou 310022, China*

Received 25 August 2018; revised 4 November 2018; accepted 28 November 2018

KEY WORDS

OCT2;
miRNA;
Renal cell carcinoma;
Epigenetic regulation;
Oxaliplatin

Abstract Renal cell carcinoma (RCC) is one of the most common malignant tumors affecting the urogenital system, accounting for 90% of renal malignancies. Traditional chemotherapy options are often the front-line choice of regimen in the treatment of patients with RCC, but responses may be modest or limited due to resistance of the tumor to anticarcinogen. Downregulated expression of organic cation transporter OCT2 is a possible mechanism underlying oxaliplatin resistance in RCC treatment. In this study, we observed that miR-489-3p and miR-630 suppress OCT2 expression by directly binding to the OCT2 3′-UTR. Meanwhile, *via* 786-O-OCT2-miRNAs stable expression cell models, we found that miRNAs could repress the classic substrate 1-methyl-4-phenylpyridinium (MPP^+), fluorogenic substrate *N*,*N*-dimethyl-4-(2-pyridin-4-ylethenyl) aniline (ASP^+), and oxaliplatin uptake by OCT2 both *in vitro* and in xenografts. In 33 clinical samples, miR-489-3p and miR-630 were significantly upregulated in RCC, negatively correlating with the OCT2 expression level compared to that in adjacent normal tissues, using tissue microarray analysis and qPCR validation. The increased binding of c-Myc to the promoter of pri-miR-630, responsible for the upregulation of miR-630 in RCC, was further evidenced by chromatin immunoprecipitation and dual-luciferase reporter assay. Overall, this study indicated that miR-489-3p and miR-630 function as oncotherapy-obstructing microRNAs by directly targeting OCT2 in RCC.

© 2019 Chinese Pharmaceutical Association and Institute of Materia Medica, Chinese Academy of Medical Sciences. Production and hosting by Elsevier B.V. This is an open access article under the CC BY-NC-ND license (http://creativecommons.org/licenses/by-nc-nd/4.0/).

*Corresponding author. Tel.: +86 571 88208407; fax: +86 571 88208407.
E-mail address: yuls@zju.edu.cn (Lushan Yu).

Peer review under responsibility of Institute of Materia Medica, Chinese Academy of Medical Sciences and Chinese Pharmaceutical Association.

https://doi.org/10.1016/j.apsb.2019.01.002
2211-3835 © 2019 Chinese Pharmaceutical Association and Institute of Materia Medica, Chinese Academy of Medical Sciences. Production and hosting by Elsevier B.V. This is an open access article under the CC BY-NC-ND license (http://creativecommons.org/licenses/by-nc-nd/4.0/).

1. Introduction

MicroRNAs (miRNAs) are a class of non-coning RNA molecules with approximately 20–25 nucleotides. They play a critical role in regulating a variety of physiological process such as cell proliferation, differentiation, and apoptosis[1]. Typically, miRNAs bind to the 3′-untranslated regions (3′-UTR) of relevant mRNA targets to negatively regulate gene expression. One miRNA may have several targets, whereas different miRNAs can bind to the same mRNA. A previous study revealed that miRNAs are pivotal regulators of cancer development and work by influencing the main cancer hallmarks[2]. In addition, miRNAs are widely present in numerous body fluids, including serum, plasma, saliva, urine, and amniotic fluid[3], making them excellent potential biomarkers for cancer diagnosis or prognosis, and recently they have become favored targets of drug development[4,5]. The development of miRNA-specific microarrays and RNA sequencing technologies has contributed to a body of evidence indicating that a range of miRNAs are dysregulated in renal cell carcinoma[6], suggesting that these may work as potential predictors of renal cell carcinoma (RCC)[7,8]. A combination treatment, with specifical antagomir or agomir of the dysregulated miRNAs, can provide insight into better and more efficacious clinical chemotherapy options[9].

Renal cell carcinoma (RCC) is one of the most common malignant tumors affecting the urogenital system, accounting for 90% of all renal malignancies[10]. The kidney carries out key metabolic processes in the body, and various drug transporters are expressed as a result. Their inactivation can lead to resistance to treatment and poor prognosis, despite better detection and subsequent treatment[11]. Results from clinical practice and trails have shown that chemotherapy treatments are often have low efficacy of around 10%–15%[12]. Patients using vascular endothelial growth factor (VEGF)-target drugs have a median overall survival time of 18.8 months, but approximately one-third of patients report grade III or grade IV adverse reactions[13]. Therefore, new targets like histone lysine-specific demethylase 1 (LSD1)[14], speckle-type POZ protein (SPOP)[15], hypoxia inducible factors (HIFs)[16], and solute carrier family 47 member 2 (*SLC47A2*)[17] are still being discovered and explored to support the development of therapeutic agents with improved toxicity and better efficacy. In a previous study, we revealed that aberrant DNA methylation at OCT2 promoter caused OCT2 repression in RCC, which drives oxaliplatin resistance in RCC[18]. Considering that miRNAs play a key regulatory role in MDR through modulating various drug resistant mechanisms[19], we hypothesized that miRNAs may also play a part in the regulation of OCT2 repression in RCC.

In this study, miRNA candidates were selected based on cross-filtering in miRNA databases. Mechanisms underlying OCT2 repression in RCC were further deciphered by validating the regulatory functions of miRNAs on OCT2 in models both *in vivo* and *in vitro*. Additionally, we studied the mechanisms of miRNA dysregulation in RCC.

2. Materials and methods

2.1. Cell culture and clinical sample collection

The 786-O, 769-P, HEK-293 cell lines were obtained from the Chinese Academy of Science Committee on type culture collection cell libraries. 786-O, 769-P cell lines were maintained at 37 °C in 5% CO_2 in RPMI 1640 medium (GIBCO, Grand Island, NY, USA) supplemented with 10% fetal bovine serum (FBS, GIBCO), 1% penicillin/streptomycin, and 1% sodium pyruvate. HEK-293 cell line was cultured with 10% FBS at 37 °C in 5% CO_2 in DMEM medium supplemented with 1% penicillin/streptomycin. To study the effect of hypoxia on gene expression, cells were cultured in anaerobic incubator (Electrotek AW400SG, UK) at 1% oxygen concentration. Surgical specimens from 33 renal cell carcinoma patients with relevant pathological information were collected from the Specimen Bank of Zhejiang Cancer Hospital (Hangzhou, China) with the approval by the Institutional Review Board of Zhejiang Cancer Hospital. Once collected, samples were immediately frozen in liquid nitrogen.

2.2. RNA extraction and quantitative real-time PCR

Total RNA from tissue samples was isolated with a total RNA mini-prep kit (Tiangen, Beijing, China) and total RNA from cell lines was isolated with an Axygen total RNA mini-prep kit. Then 500 ng RNA was reverse transcribed to cDNA with PrimeScript® RT Master Mix (DRR036A, Takara, Japan) for gene expression analysis and specific primers were used to reverse transcribe RNA with PrimeScript® RT Master Mix (DRR037A, Takara) for miRNAs analysis. Quantitative real time PCR was performed with SYBR® Premix EX Taq (Takara) in StepOnePlus Real-Time PCR System (StepOnePlus). Specific primers were listed in Supporting Tables. The relative expression level of transcripts was measured by normalization to GAPDH in both cell lines and patient tissues.

2.3. Luciferase assay

Wild type or mutated OCT2 3′-UTR were homologous recombined to PGL3 promoter vector (Promega, Wisconsin, USA) for the construction of reporter plasmids. OCT2 3′-UTR mutants were obtained through directly deleted with PCR, primers listed in Supporting Information Table S1. A 2-kb region upstream of miR-630 TSS was cloned into a luciferase pGL3-basic vector, cotransfecting HEK293 cells with c-Myc expression plasmid or empty expression vector (pENTER). Luciferase assay was performed following standard protocols, as described previously[18]. Briefly, cells were transfected with plasmids using Lipofectamine® 2000 for HEK293 cells. Twenty-four hours after transfection, cells were harvested and subjected to luciferase assay using Dual-Luciferase® Reporter Assay System (Promega, Wisconsin, USA) according to the manufacturer's protocol.

2.4. Western blot analysis

Western blot was performed following standard protocols, detailed as follows: cells were harvested and lysed using RIPA buffer (Beyotime, Shanghai, China). Protein extracts were subjected to SDS-PAGE analysis. The membranes were blocked with 5% BSA buffer followed by antibody hybridization and then visualized in G-BOX gel imaging system (Chemi XR 5, Syngene, Cambridge, UK).

2.5. Cellular uptake assays

N,*N*-Dimethyl-4-(2-pyridin-4-ylethenyl) aniline (ASP^+) and 1-methyl-4-phenylpyridinium (MPP^+), two classical substrate of human OCT2, were used to detect the OCT2 transport capacity. The cells were seeded into 24-well plates. After 48 h, the culture

medium was replaced with 200 μL Hanks balanced salt solutions (HBSS) containing inhibitors at 37 °C for 10 min as pre-incubation. Then the solution was aspirated off and replaced with 200 μL of HBSS containing ASP^+ or MPP^+. The concentration of ASP^+ and MPP^+ were 5 and 10 μmol/L, respectively. Incubation process lasted for 3 min and then washed wells with ice cold PBS. The cells were lysed with 100 μL 0.1% sodium dodecyl sulfonate (SDS, Sigma, St. Louis, MO, USA) and pipetted up and down 30 times per well. Before uptake analysis, miRNA mimics and inhibitors were transinfected into cells to overexpress or depress miRNAs.

Cells incubated with ASP^+ can directly analyze fluorescence in Spectra Max M2 Microplated Reader (Molecular Devices, San Jose, CA, USA) at excitation wavelength of 475 nm and absorption wavelength of 605 nm. Cells incubated with MPP^+ need to be lysed for LC–MS analysis. LC–MS method was detailed previously[20].

2.6. Construction of stable expressed cell lines

786-O-OCT2-630 and 786-O-OCT2-489 stably expressed cell lines were constructed for further research. OCT2-CDS-3′-UTR-pCDH plasmid was used for lentiviral transfection to overexpress OCT2. MiR-630 or miR-489-3p lentiviral vector were used for second lentiviral transfection to overexpress miRNAs. Vectors were purchased from Vigene Biosciences (Rockville, MD, USA). After transinfected, cells were selected with 0.5 μg/mL puromycin for a week and then observed in Ti-S Fluorescence Inversion Microscope System (Nikon, Japan). Cells were performed uptake assays to ensure its transport function.

2.7. MTT assay

Cells were seeded into 96-well plates at 3×10^4 cells per well in 100 μL of supplemented medium. After 24 h, medium was replaced by fresh medium with oxaliplatin (Sigma) in concentration gradient (0–250 μmol/L). After 24 h, medium was replaced by fresh one. Cells were incubated for another 24 h and then added 100 μL fresh medium with 0.5 mg/mL MTT (Solarbio, Beijing, China), incubating at 37 °C for 4 h and discarding the medium. Then 100 μL DMSO was added and shaken at 37 °C for 30 min. The optical density was measured at 570 nm wavelength and the data were expressed as a percentage of control density.

2.8. Platinum quantification by ICP–MS

Cells were incubated at 37 °C in the presence of oxaliplatin (100 μmol/L) for 48 h. Cells were washed twice with ice cold PBS and collected by centrifugation. A small amount of cell pellet was taken for cell counting. Genomic DNA was extracted from cell pellets or dissected tumors using blood/cell/tissue genomic DNA extraction kit (TIGEN, Beijing, China) as manufacture protocol described. After quantification, DNA was extracted with phenol chloroform extraction and precipitated using 70% of ethanol. Cell pellets or DNA pellets were digested as described. The amount of platinum in samples was determined by inductively coupled plasma mass spectrometry (ICP-MS, Idiscover Co., Ltd., Hangzhou, China).

2.9. Xenograft studies

Animals were randomly assigned to groups based on relative tumor volume and were euthanized at the end of the study. All mouse experiments followed institutional guidelines and were approved by Zhejiang University Animal Care and Use Committee (Hangzhou, China). Each female BALB/c nude mouse (National Rodent Laboratory Animal Resource, Shanghai, China) was injected subcutaneously with 10^7 786-O-pCDH, 786-O-OCT2-NC, 786-O-OCT2-489 or 786-O-OCT2-630. When the mean tumor size reached 100 mm^3, mice were administered with oxaliplatin intraperitoneally (10 mg/kg for 786-O xenografts) every 10 days for total 3 times. Tumor sizes and animal weights were monitored. Tumor volumes were calculated as follow: $L \times W^2/2$, where L and W is the longest and shortest dimension, respectively. All mice were euthanized at Day 26.

2.10. Chromatin immunoprecipitation (ChIP) assay

ChIP experiments were carried out as described[18]. Primers used in ChIP-qPCR are listed in Supporting Information Table S2. Enrichment was normalized to total input. ChIP grade antibodies including anti-OCT2 (Sigma, HPA008567-100UL), anti-H3 (Abcam, ab1791), anti-c-Myc (Abcam, ab32072) and normal rabbit IgG (Santa Cruz Biotechnology, sc-2027) were used in this study.

2.11. miRNA in vivo precipitation (miRIP)

Biotin-labeled *OCT2* mRNA probes, synthesized and purchased from RiboBio Co., Ltd. (Guangzhou, China), were transfected into 786-O-OCT2-489 and 786-O-OCT2-630 to hybridize *OCT2* mRNA for 48 h. Biotech and the miRIP assay were performed as previously described[43] with minor modification. Cells were fixed by 1% formaldehyde for 10 min, lysed and sonicated (QSONICA-Q800R2) using the following parameters: 50% amplitude, 30 s constant pulse, and 30 s pause. After centrifugation, 50 μL of the supernatant was retained as input and the remaining part was incubated with pretreated streptavidin dynabeads (86031, Polyscience, Niles, IL, USA) at room temperature (RT) for 2 h. Then the mixture was washed and incubated with 200 μL lysis buffer for 2 h at RT. Finally, the RNA was extracted with TRIZOL (Sigma) for further detection.

2.12. Exosomes isolation and characterization

Exosomes were obtained from culture medium as previously described with some modification[44]. In brief, cells were grown in RPMI 1640 media supplemented with 10% exosome-free FBS. Next, the media was collected and centrifuged at $300 \times g$ for 10 min to pellet cells, followed by a centrifugation step of $2000 \times g$ for 15 min to discard dead cells, and a centrifugation of $10{,}000 \times g$ for 30 min to discard cell debris. The supernatant was filtered through a 0.22 μm pore filter (syringe filter, SLGP033RS, Millipore, USA). This was followed by two ultracentrifugations at $100{,}000 \times g$ for 70 min to pellet the exosomes. All spins were performed at 4 °C.

Exosomes were resuspended by PBS (02-024-1A, Biological Industries, Israel) and then examined by Electron Microscopy using negative staining. Exosomes used for protein immunoblotting were resuspended in PBS, quantified by bicinchoninic acid assays

(P0011, Beyotime) and mixed with SDS loading buffer (C516031, Sangon Biotech, China). Exosomes used for size distribution were resuspended and diluted in PBS, then analysed by ZetaView (Particle Metrix, Germany). Exosomes used for RNA extraction were resuspended in 700 μL of QIAzol Lysis Reagent (79306, QIAGEN) and processed as the protocol of miRNeasy Micro Kit (217084, QIAGEN).

2.13. Statistical analysis

Statistical analysis was performed using Graphpad Prism 5 (Graphpad Softwear, La Jolla, CA, USA). Image J was used for western blot grayscale analysis. Spearman correlation analysis was used to analyze correlation of OCT2 expression change and miRNAs expression change. Student's *t*-test was used to compare experimental groups with controls. P values <0.05 were considered statistically significant. All statistical analyses were expressed as mean ± S.E.M. (standard error of mean).

3. Results

3.1. MiR-489-3p and miR-630 directly target OCT2

To determine the specific miRNAs that may be involved in the downregulation of OCT2, we performed an analysis using data from publicly available miRNA target prediction databases (Fig. 1A). The candidate targets selected were miR-630 (according to "miRBase", just one mature sequence processed from the 3′ end of pre-miR-630 was reported), miR-155-5p, miR-489-3p, miR-181a-5p, miR-431-5p, and miR-488-3p, using TargetScan, miRanad, and microcosm, integrated with miRNA arrays which compare miRNA expression between RCC tumor and matched adjacent non-tumor tissues. To examine whether the selected miRNAs directly target OCT2, a segment of the OCT2 3′-UTR was cloned into a luciferase pGL3-promoter vector at the end of 3′ of the luciferase open-reading frame (pGL3-OCT2 3′-UTR). Compared with the scrambled miRNA-transfected control (NC), luciferase activity was significantly decreased in HEK-293 cells (which do not exhibit endogenous OCT2 and miR-489-3p or miR-630 expression) cotransfected with miR-489-3p or miR-630 mimic and pGL3-OCT2 3′-UTR plasmid, together with the renilla luciferase plasmid. No significant alteration in luciferase activity was observed in cotransfections with other candidate miRNA mimics (Fig. 1B). Bioinformatic analyses revealed the putative miR-489-3p miRNA recognition element (MRE) at a position of 448–454 base pairs (bp) downstream of the OCT2 stop codon. There were two putative MREs for miR-630 corresponding to 315–322 bp and 559–565 bp respectively, within the 3′-UTR of OCT2 (Fig. 1C). To confirm that the inhibition of luciferase activity was due to miR-489-3p and miR-630 binding to their respective binding sites, a 6-bp deletion mutation was created at the MRE seed sequence within the pGL3-OCT2 3′-UTR (termed mutant pGL3-OCT2 3′-UTR). The significantly decreased luciferase activity between NC and miR-489-3p in HEK-293 cells, cotransfected with pGL3-OCT2 3′-UTR, was partially reversed by cotransfecting with mutant pGL3-OCT2 3′-UTR (Fig. 1D). Given that two miR-630 MREs distributed at different locations in OCT2 3′-UTR, deleted either did not affect luciferase activity inhibition by miR-630, while mutated both simultaneously, the inhibitory effect was negligible (Fig. 1E). To compare the inhibitory effect of miR-489-3p and miR-630 on OCT2 3′-UTR luciferase activity, HEK-293 cells were separately or synchronally transfected with 10 μmol/L miR-489-3p and 5 μmol/L miR-630, together with pGL3-OCT2 3′-UTR and a renilla luciferase plasmid. Compared with miR-489-3p, miR-630 can better suppress luciferase activity at a lower concentration (Fig. 1F).

3.2. MiR-489-3p and miR-630 suppress OCT2 expression and activity

Endogenous OCT2 expression in kidney cancer cells is generally low. OCT2 transcription can be activated in RCC cell lines under treatment with decitabine (DAC), a demethylating reagent that globally inhibits DNA methylation by blocking cellular DNA methyltransferases (DNMTs)[18]. To address whether miR-489-3p and miR-630 contribute to RCC multidrug resistance (MDR) through modulating the expression of OCT2, we transiently transfected miR-489-3p and miR-630 mimics in 786-O and 769-P cells treated with 2.5 μmol/L DAC for 72 h. Overexpression of miR-489-3p and miR-630 downregulated *OCT2* mRNA and protein expression levels, as well as the uptake of 1-methyl-4-phenylpyridinium (MPP^+) and *N*,*N*-dimethyl-4-(2-pyridin-4-ylethenyl) aniline (ASP^+), two classical substrates of human OCT2[20], in 786-O and 769-P cells (Supporting Information Fig. S1). Further to this, a fragment containing CDS and 3′-UTR of OCT2 was inserted into a lentivector pCDH-EF1-MCS-T2A-copGFP. Virus packaging and stable cell selection were performed on 786-O cells to construct an OCT2 stably expressing cell line (termed 786-O-OCT2). Compared with cells transfected with the parent vector (786-O-pCDH), both mRNA and protein expression levels and the uptake of MPP^+ in 786-O-OCT2 were significantly upregulated (Fig. 2B–D). Next, the full-length cDNA of pre-miR-489-3p, pre-miR-630 and NC were prepared and inserted into a lentivector pLent-U6-RFP-Puro to construct cell lines stably overexpressing miR-489-3p and miR-630, respectively (termed 786-O-OCT2-NC, 786-O-OCT2–489, 786-O-OCT2–630), after virus packaging and stable cell selection with 0.5 μg/mL puromycin on 786-O-OCT2. The expression level of miR-489-3p, miR-630 and the fluorescence intensity were detected in each cell model. The well overlapped red fluorescence and green fluorescence, and upregulation of miR-489-3p and miR-630 compared with 786-O-OCT2-NC, indicated the successful construction of the cell lines that stably overexpressing OCT2 and miRNAs simultaneously (Fig. 2A and E). Like DAC-induced renal cancer cells, overexpression of miR489-3p and miR-630 in OCT2 stably overexpressed cells resulted in inhibition of OCT2 RNA, protein expression level, and uptake ability of MPP^+, compared to those in 786-O-OCT2-NC cells (Fig. 3A–C). Conversely, down regulation of miR-489-3p and miR-630 by transiently transfected 100 nmol/L miR-489-3p or miR-630 inhibitor in 786-O for 36 h rescued *OCT2* mRNA levels by 2.5- and 3.5-fold compared with microRNA inhibitor NC. The increase in *OCT2* mRNA levels corresponded with significant increases in MPP^+ accumulation (Fig. 3D–F). To further verify the binding of miR-489-3p and miR-630 to OCT2 in renal cancer cells, four special *OCT2* mRNA antisense oligonucleotides with 3′ biotin-tagged were designed to precipitate miRNAs binding to *OCT2* mRNA in 786-O-OCT2-489 and 786-O-OCT2-630 cell lines (Fig. 3G). RT-PCR analysis on the mRNA extractions of *OCT2* mRNA probes transfected cells demonstrated a specific enrichment for the mRNA of *OCT2* compared with input. The enriched

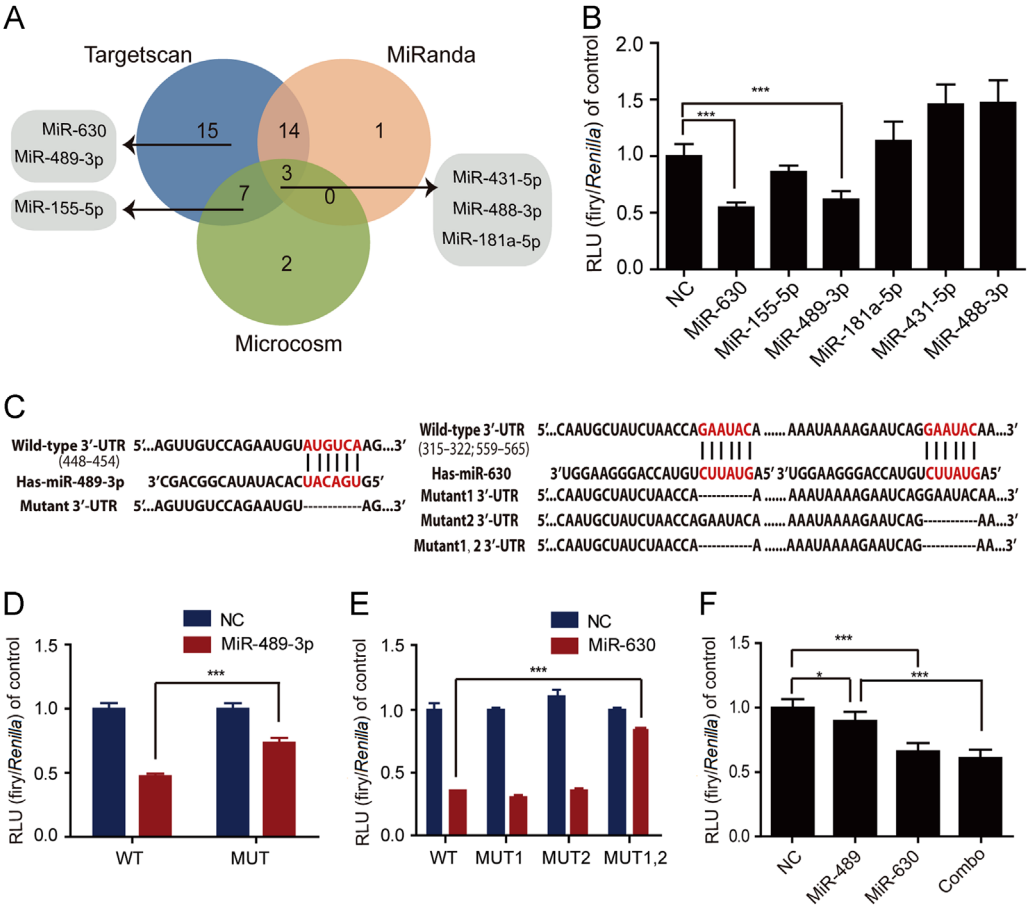

Figure 1 MiR-489-3p and miR-630 directly target OCT2. (A) Summary of miRNAs potentially target OCT2 3′-UTR. (B) Dual-luciferase reporter gene assay in HEK293 cells cotransfected with miRNA mimics and wild-type pGL3-OCT2 3′-UTR plasmid together with the *Renilla* luciferase plasmid. (C) MiR-489-3p, miR-630 and their putative binding sequences in the 3′-UTR of OCT2. A 6-bp deletion mutation was generated in the complementary site that binds to the seed region. (D) and (E) Dual-luciferase reporter gene assay in HEK293 cells cotransfected with miRNA mimics and mutant pGL3-OCT2 3′-UTR plasmid (seed deletion of miR-489-3p and miR-630 separately). (F) Dual-luciferase reporter gene assay in HEK293 cells separately or synchronally transfected with 10 μmol/L miR-489-3p and 5 μmol/L miR-630 together with pGL3-OCT2 3′-UTR and *Renilla* luciferase plasmid. Student's *t*-test (two-tailed) was used. Data are the mean ± S.E.M ($n=6$). $^{*}P<0.05$, $^{***}P<0.001$.

miR-489-3p and miR-630 were also detected and were confirmed to interact with OCT2 (Fig. 3H and I).

3.3. *MiR-489-3p and miR-630 promote chemoresistance to oxaliplatin in RCC cells*

Oxaliplatin, a platinum-based chemotherapeutic agent, is mainly transported into cells by OCT2. To investigate the contribution of miR-489-3p and miR-630 to chemoresistance to oxaliplatin in renal cancer cells, 786-O-pCDH, 786-O-OCT2-NC, 786-O-OCT2-489 and 786-O-OCT2-630 cell lines were treated with 100 μmol/L oxaliplatin for 48 h. The intra-cellular Pt accumulation, detected *via* ICP-MS, indicated stable expression of OCT2 and increased oxaliplatin uptake (by 2.5-fold), which can be suppressed by miR-489-3p and miR-630 (Fig. 4A). Accordingly, overexpression of OCT2 significantly decreased the growth-inhibitory effect of oxaliplatin in 786-O cells after being treated with different concentrations of oxaliplatin (0–250 μmol/L) for 48 h, as measured by MTT assay (The IC_{50} values of 786-O-pCDH, 786-O-OCT2-NC, 786-O-OCT2-489 and 786-O-OCT2-630 were 68.09, 36.00, 57.94, and 60.47 μmol/L, respectively). In contrast, overexpression of miR-489-3p or miR-630 reversed the up-regulated sensitivity to oxaliplatin (Fig. 4B). To simulate the inhibitory effect of miR-489-3p and miR630 on OCT2 *in vivo*, a xenograft mouse model was established to monitor the therapeutic effect of oxaliplatin. The timeline of oxaliplatin administration is shown in Fig. 4C. Two weeks after administration, the tumors from four nude mice, randomly selected from each group, were resected and examined *via* PT-PCR, to verify that the expression of *OCT2* and miRNA remained in an over-expressed state (Supporting Information Fig. S2). Regarding tumor growth, mice bearing tumors originating from 786-O-OCT2 cells demonstrated a remarkably delayed tumor growth, or even tumor shrinkage, with prolonged administration compared with 786-O-pCDH cells. By contrast, overexpression of miR-489-3p or miR-630 in 786-O-OCT2 cells enhances its resistance to oxaliplatin and accelerates tumor growth in the xenograft model (Fig. 4D and E). At 26 days after administration, the mice in each group were sacrificed and the tumors were resected to determine the OCT2 protein expression level and platinum accumulation (Fig. 4F and G). Compared to the drastic decline in OCT2 protein expression and platinum accumulation in the miRNA-overexpression groups, no significant difference in *OCT2* expression was detected at the mRNA level (data not shown), which may be because post-transcriptional suppression of OCT2 by

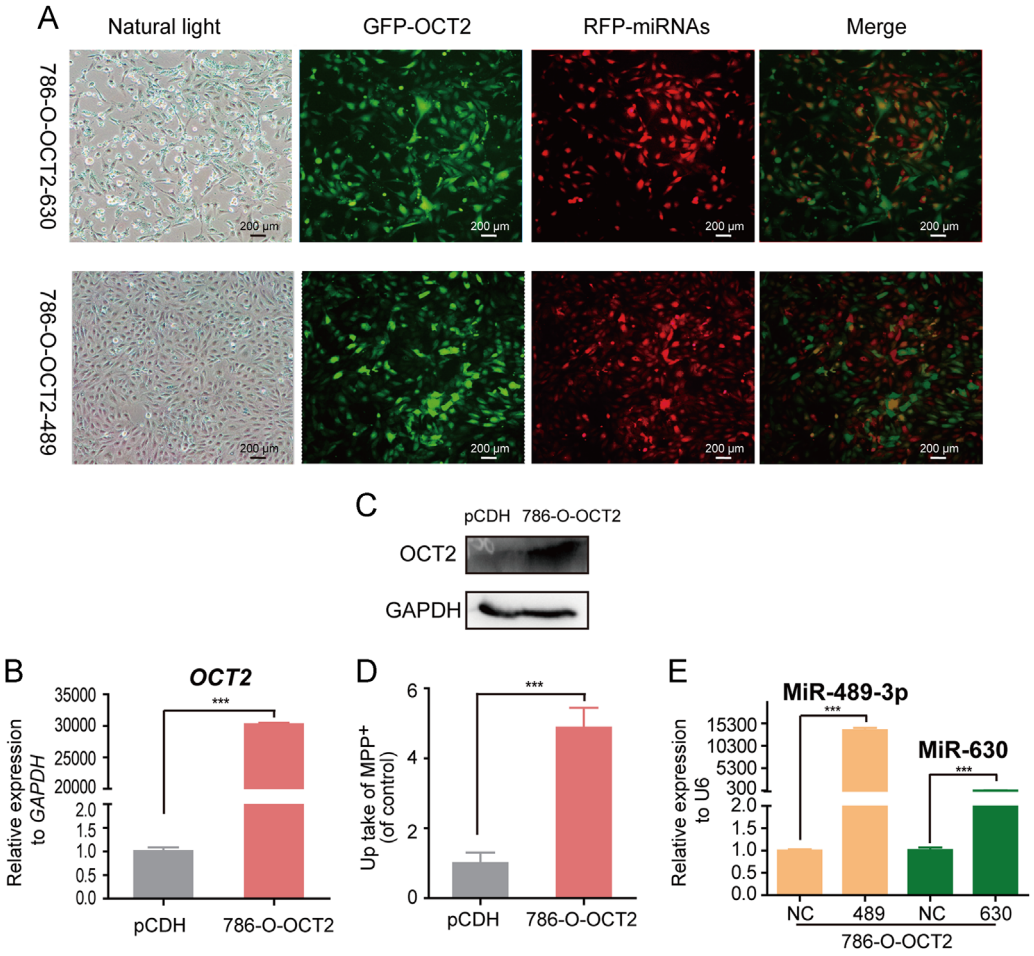

Figure 2 Construction of 786-O cell line, stably overexpressing of OCT2, together with miR-489-3p or miR-630. (A) The fluorescence intensity in 786-O-OCT2-489 and 786-O-OCT2-630. Green fluorescence indicates overexpression of OCT2 while red fluorescence indicates miRNAs overexpression. (B)–(D) Upregulation of *OCT2* mRNA and protein expression level and the uptake of MPP^+ in 786-O-OCT2 compared with 786-O-pCDH. (E) Detection of miR-489-3p and miR-630 expression level by qRT-PCR, with U6 as an endogenous control, in 786-O-OCT2-489, 786-O-OCT2-630 and 786-O-OCT2-NC.

miR-489-3p and miR-630 is dominant *in vivo*. Together we conclude that epigenetic suppression of OCT2 by miR-489-3p and miR-630 reduces intracellular platinum accumulation and consequently enhances chemoresistance of RCC cells to oxaliplatin, both *in vitro* and in xenografts.

3.4. *MiR-489-3p and miR-630 are overexpressed in RCC*

Previous research from our lab demonstrated that OCT2 is repressed at both mRNA and protein expression levels in RCC. MiR-489-3p and miR-630 were also found to be uniquely upregulated in RCC, *via* microarray analysis and RT-PCR verification[21,22]. To confirm the expression dysregulation of miR-489-3p and miR-630 in RCC, expression of *OCT2*, miR-489-3p and miR-630 was evaluated by RT-PCR in human matched renal normal-tumor samples ($n=33$). As the expression of miR-630 in some tissues is below the detection limit, 15 pairs of tissue were selected for miR-630 analysis (Fig. 5A). We also classified tissue samples according to age, gender, cancer type and TNM stage of patients. We concluded that those patients with clear cell renal cell carcinoma (ccRCC) as well as TNM class I tend to have elevated miR-489-3p and miR-630 expression, which enables both miRNAs to be considered as biomarkers for early diagnostic and pathomorphological classification (Fig. 5B). Following this, we investigated the expression level of miR-489-3p and miR-630 in human proximal tubule epithelial cell line HK-2 and human RCC cell lines. By qRT-PCR, we showed that the expression of both miR-489-3p and miR-630 was significantly upregulated in 786-O, 769-p, and CAKI cancer cell lines compared to HK-2 cells (Fig. 5C).

3.5. *C-Myc upregulates miR-630 by binding to its promoter region*

We next attempted to identify the mechanisms that underlie miR-489-3p and miR-630 upregulation in RCC. Considering that the biogenesis of miRNA is a multistep process, and each of these steps is potentially subjected to regulation, we detected the expression of Drosha, exportin-5 (*XPO5*), Dicer and *AGO2*, all key enzymes in human miRNA biogenesis[23,24] using RT-PCR. No significant expression difference at mRNA level was found in human matched renal normal-tumor samples (Supporting information Fig. S3). Previously, we found that c-Myc plays an important role in the regulation of OCT2 expression by interacting with the E-Box motif. Overexpression of c-Myc is estimated to occur in 70% of human tumors[25], which was verified here in human matched renal normal-tumor samples by RT-PCR ($n=10$) and Western blot ($n=5$) (Fig. 6A and B). To test whether c-Myc

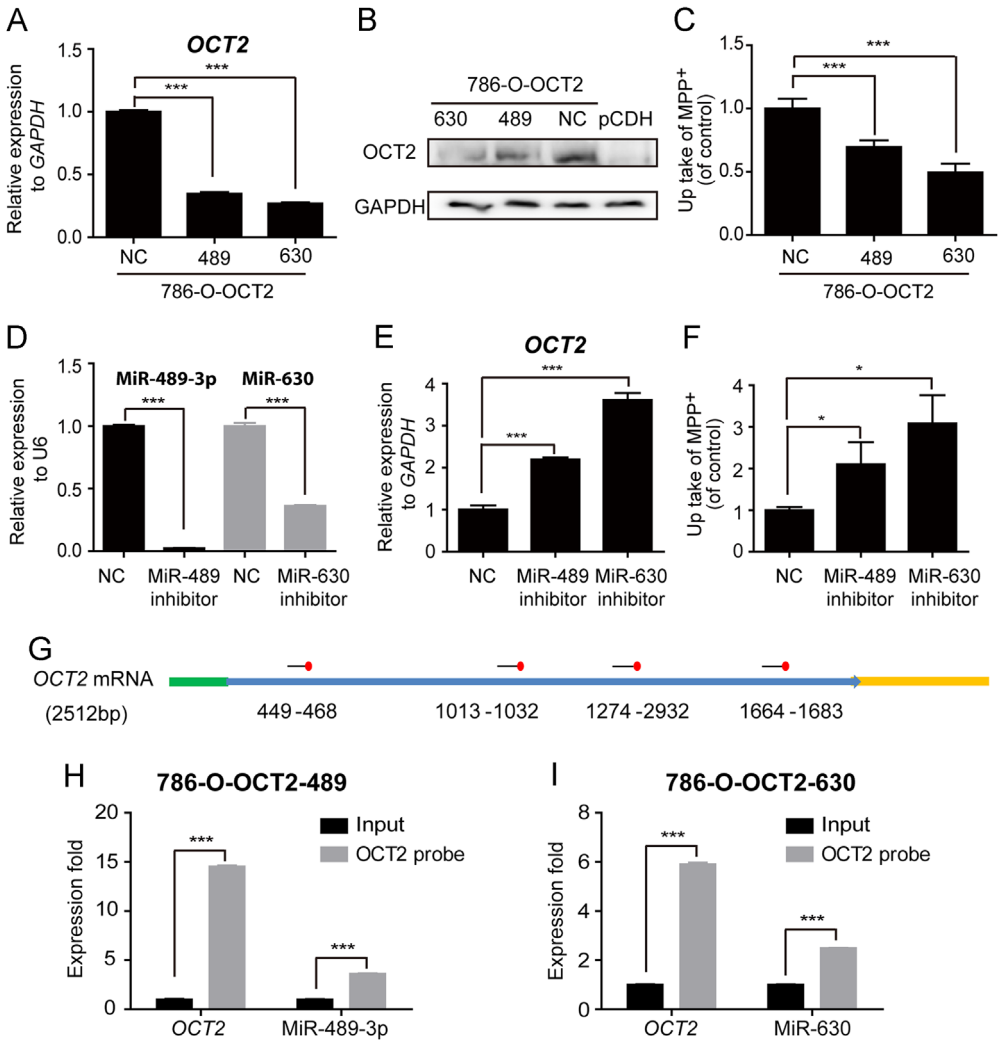

Figure 3 MiR-489-3p and miR-630 suppress OCT2 expression and activity. (A)–(C) Downregulation of *OCT2* mRNA, protein expression levels and the accumulation of MPP^+ in 786-O-OCT2-489, 786-O-OCT2-630 compared with 786-O-OCT2-NC. 100 nmol/L of microRNA inhibitor NC, miR-489-3p or miR-630 inhibitor were transiently transfected into 786-O cells for 48 h: (D) Quantitative analysis of endogenous mature miR-489-3p and miR-630 expression levels were measured by qRT-PCR with U6 as an endogenous control. (E)–(F) The mRNA expression level of *OCT2* and uptake of MPP^+ were measured by qRT-PCR and LC–MS. (G) *OCT2* mRNA and probe binding sites. The green bar, 5′-UTR; the blue arrow, coding sequence; the yellow bar, 3′-UTR; the black bars and the numbers at the bottom denote regions the probe binding sites; the red balls indicate where biotin binded. (H)–(I) OCT2, miR-489-3p and miR-630 in 786-O-OCT2-489 and 786-O-OCT2-630 cell lysis was pulled down and enriched with OCT2 specific probes and then detected by qPCR.

can act as a transcriptional activator, promoting transcription expression of miRNAs, PROMO bioinformatics software was utilized to analyze a 2-kb region upstream of the transcription start site (TSS) of miR-489-3p and miR-630. Two c-Myc binding motifs (E-Box: CACGTG) were identified inside the putative miR-630 promoter region named E1 (–1638 to –1632) and E2 (–1034 to –1040) (Supporting Information Fig. S4). In addition, we transfected specific pri-miR-630, primary miRNA transcript of miR-630, siRNA into 786-O cells and found that the expression of pre-miR-630, precursor miRNA of miR-630, and miR-630 were simultaneously reduced, while *OCT2* was slightly elevated (Fig. S4). These results suggest that the abnormal up-regulation of miR-630 in RCC was mediated by increased pri-miR-630. We then examined whether global upregulation of c-Myc was responsible for the transcriptional regulation of miR-630 expression. The 786-O cells were pretreated with doxycycline at 1 μg/mL for 72 h to turn on the expression of specific c-Myc knockdown ShRNA. The expression of pri-miR-630 and pre-miR-630 was suppressed, accompanied with upregulation of *OCT2* mRNA and uptake of MPP^+ in c-Myc depleted 786-O cells, suggesting that c-Myc is an upstream regulator of miR-630 (Fig. 6C and D). Using RT-PCR assay, we were also able to show that overexpression of c-Myc promoted pri-miR-630 expression (Fig. S4). Chromatin immunoprecipitation (ChIP) assays performed on the above-mentioned c-Myc knockdown cell model and 786-O cells that transiently transfected with c-Myc expression plasmid or empty expression vector (pENTER) demonstrated that c-Myc mainly occupied around E2 fragment and the abundance was positively correlated with its expression level (Fig. 6E). A human matched renal normal-tumor samples, overexpressed with c-Myc and

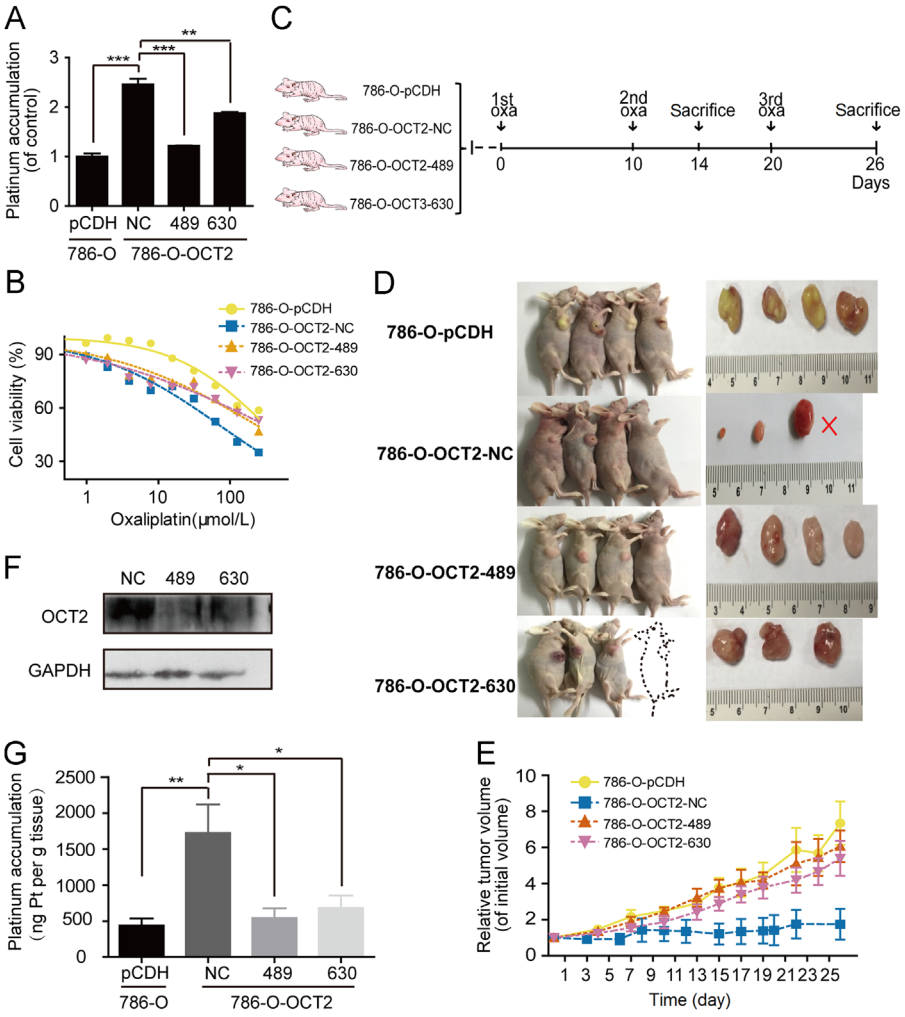

Figure 4 MiR-489-3p and miR-630 promote chemoresistance to oxaliplatin in RCC cells. (A) Overexpression of OCT2 increased oxaliplatin cellular accumulation which can be suppressed by miR-489-3p and miR-630. (B) The cell viability of 786-O-pCDH, 786-O-OCT2-NC, 786-O-OCT2-489 and 786-O-OCT2-630 treated with different concentrations (0–250 μmol/L) of oxaliplatin for 48 h. C) Oxaliplatin administration timeline and experiment schedule for xenograft models. The *in vivo* effect of miR-489-3p and miR-630 was evaluated in xenograft models bearing tumours originating from 786-O-pCDH, 786-O-OCT2-NC, 786-O-OCT2-489 and 786-O-OCT2-630 cell lines, $n=5$/group. In the middle of administration timeline, a mouse randomly selected from each group ($n=1$) was sacrificed to detect the expression of *OCT2*, miR-489-3p and miR-630. (D) Representative images of mice bearing xenografts and tumours after resection from each group at day 26. In 786-O-OCT2-630 model, the mouse drawn in dashed line represents one which was euthanized when tumour size reached 1500 mm^3 at day 19. In 786-O-OCT2-NC model, "×" indicates that the tumour in one mouse eventually disappeared. (E) Tumour volume was periodically measured for each mouse and tumour growth curves were plotted. Data are means ± S.E.M. ($n=4$), except for the one in 786-O-OCT2–630 model, euthanized ahead of the end point for bearing oversized tumour. (F) and (G) OCT2 protein expression level and platinum accumulation in tumours resected from each group ($n=3$).

pri-miR-630, further confirmed that higher abundance of c-Myc occupied around E2 in RCC compared with adjacent nontumor tissue (Fig. 6F). To further determine the occupancy of c-Myc on E2 element activated miR-630 expression, a 2-kb region upstream of miR-630 TSS was cloned into a luciferase pGL3-basic vector, cotransfecting HEK293 cells with c-Myc expression plasmid or pENTER. A dual luciferase reporter assay demonstrated that c-Myc binds to the promoter sequences of miR-630 containing CACGTG element. After E2 element deletion, luciferase activity was reduced to the basal level (Fig. 6G). Together we conclude that the aberrant upregulation of miR-630 was partly due to the enrichment of c-Myc at E2 motif of miR-630 promoter in RCC.

3.6. Potential of miR-489-3p and miR-630 as candidate biomarkers

Recently, there are more and more studies revealed that exosomes may play important roles in cancer. To investigate whether miR-489-3p and miR-630 can be secreted through exosomes and used as biomarkers, we isolated exosomes from culture media of three stable transfected cell lines (786-O-OCT2-NC, 786-O-OCT2–489 and 786-O-OCT2–630). The typical cup-shaped particles ranging from 30 to 150 nm in diameter was identified by electron microscopy using negative staining method (Fig. 7A). Nanoparticle tracking analysis through ZetaView showed a consistent size distribution of exosomes (Fig. 7B). In addition, western blot analysis further verified

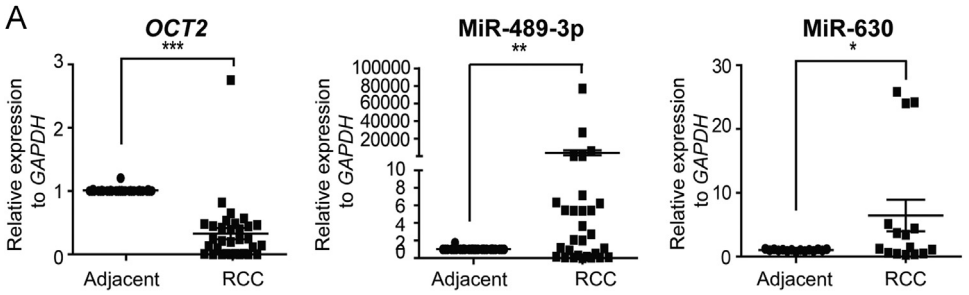

B

Variable	Total	*OCT2* downregulation	MiR-489-3p upregulation
Age			
≤30	1	—	1
30-50	5	5	2
≥50	27	27	15
Gender			
Male	23	22	12
Female	10	10	6
Type			
ccRcc	24	24	14
chRcc	4	4	3
pRcc	1	—	1
Others	4	4	0
TNM			
I	29	29	18
>I	4	4	0

Variable	Total	*OCT2* downregulation	MiR-630 upregulation
Age			
30-50	3	3	2
≥50	12	12	8
Gender			
Male	10	10	6
Female	5	5	4
Type			
ccRcc	7	7	6
chRcc	4	4	3
pRcc	1	1	0
Others	3	3	1
TNM			
I	12	12	9
>I	3	3	1

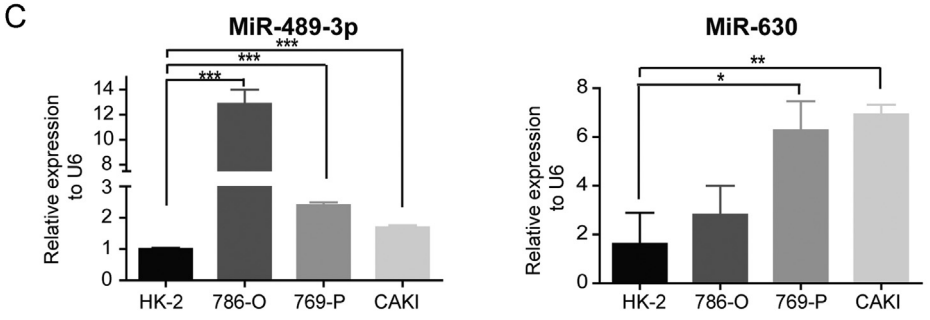

Figure 5 MiR-489-3p and miR-630 are overexpressed in RCC. (A) Comparison of *OCT2*, miR-489-3p and miR-630 expression separately in human matched renal normal-tumour samples ($n=33$, for the expression of miR-630 in some tissues is below the detection limit, $n=15$ for miR-630 analysis). Wilcoxon signed rank test was used, $^{*}P<0.05$, $^{**}P<0.01$, $^{***}P<0.001$. (B) Association between the expression level of *OCT2*, miR-489-3p, miR-630 and clinic pathological characteristics of RCC patients. (C) MiR-489-3p, miR-630 expression in renal cancer cells 786-O, 769-P and CAKI compared to normal renal epithelial cells HK-2. U6 was used as an internal control.

the characteristic exosomal protein ALIX, TSG101 and CD63 were presented in the isolated particles. Meanwhile, the exosome-excluded endoplasmic reticulum protein GRP94 was hardly detectable in the isolated particles, but abundant in the cell lysis (Fig. 7C). Above results confirmed that the isolated particles were exosomes. Then exosomal miRNAs derived from three stable transfected cell lines were extracted, reverse transcribed and quantitated by Real-Time PCR System. As shown in Fig. 7D, compared to negative control, there was a high level of exosomal miR-489-3p or miR-630 in each miRNA stable transfected cell line respectively. Interestingly, the enrichment of exosomal miR-489-3p and miR-630 were more significant than the cellular level, which suggested that dysregulated miRNAs may be secreted through exosomes in ccRCC cells.

4. Discussion

Our data show that miR-489-3p and miR-630 are significantly upregulated in RCC tissue, consistent with previous studies[21,22]. Conventionally, invasive biopsy, which has a limited success rate and raises a number of complications, is available to confirm the identity of renal masses and detect aberrant miRNA expression.[26] A recent study indicated that miRNAs are present in numerous body fluids, including serum, plasma, saliva, urine, and amniotic fluid[3]. Wang et al.[27] showed a significant increase of miR-197a-3p, miR-362, and miR-572 and a marked decrease of miR-378 and miR-28-5p in the serum of RCC patients compared to those in normal volunteers. We also examined the expression of miR-489-3p and miR-630 in plasma samples of ccRCC patients.

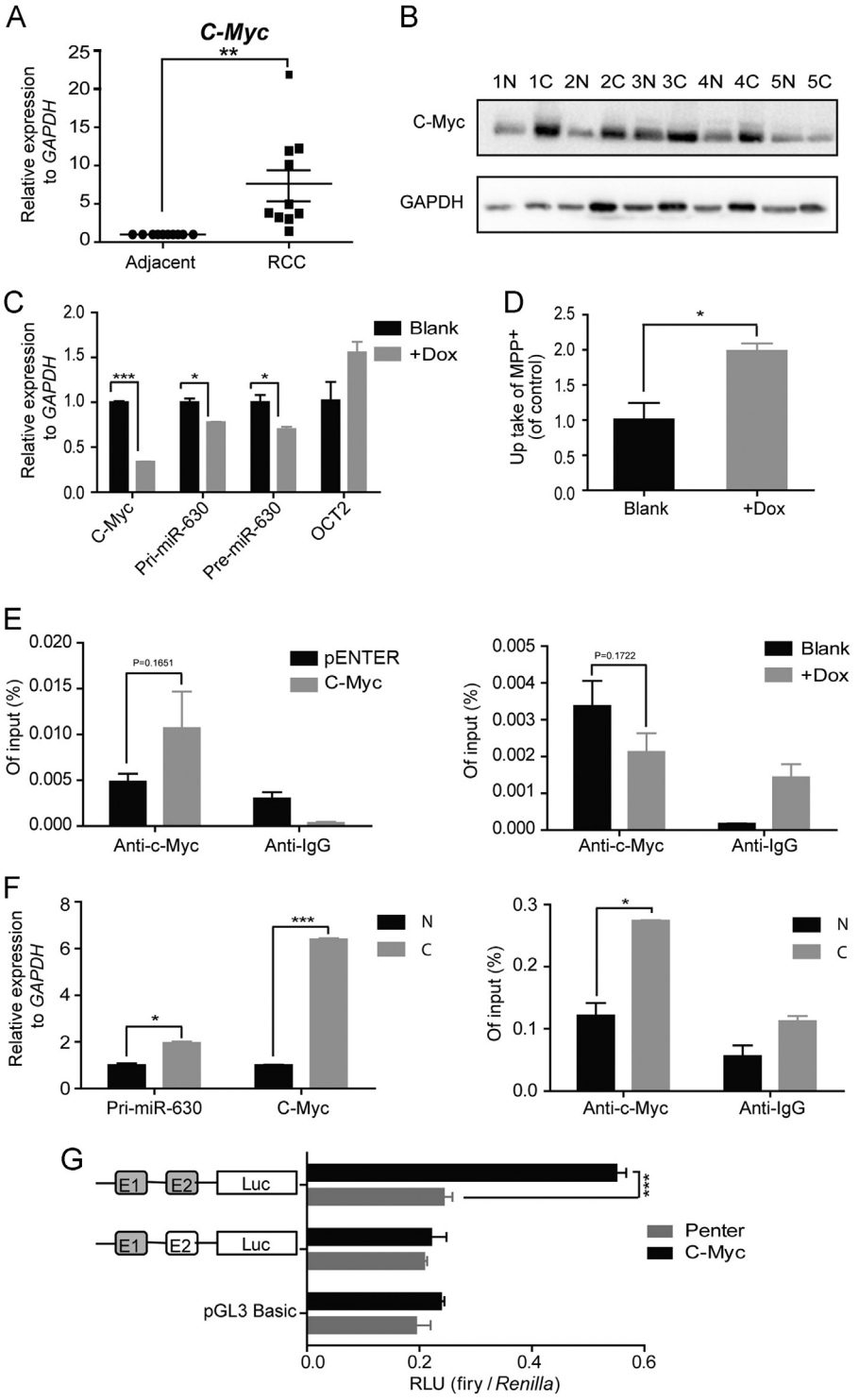

Figure 6 C-Myc upregulates miR-630 expression by binding to its promoter region. (A) and (B) Comparison of *C-Myc* mRNA and protein expression in human matched renal normal-tumour samples. (C) The expression of *C-Myc*, pri-miR-630, pre-miR-630 and *OCT2* in c-Myc knockdown 786-O cells. (D) The uptake of MPP^+ in c-Myc knockdown 786-O cells. (E) Chip-qPCR analysis of c-Myc at the promoter of miR-630 in c-Myc knockdown cell model and 786-O cells that transiently transfected with c-Myc expression plasmid or empty expression vector (pENTER). IgG, immunoglobulin G. (F) The expression of *C-Myc*, pri-miR-630 and abundance of c-Myc occupied around E2 in human matched renal normal-tumor samples. (G) Relative light unit (RLU) was detected in HEK293 cells transfected with wild pri-miR-630 promoter (gray) or E-Box element (CACGTG) mutated (white) reporter plasmid along with either c-Myc or empty expression vector (pENTER).

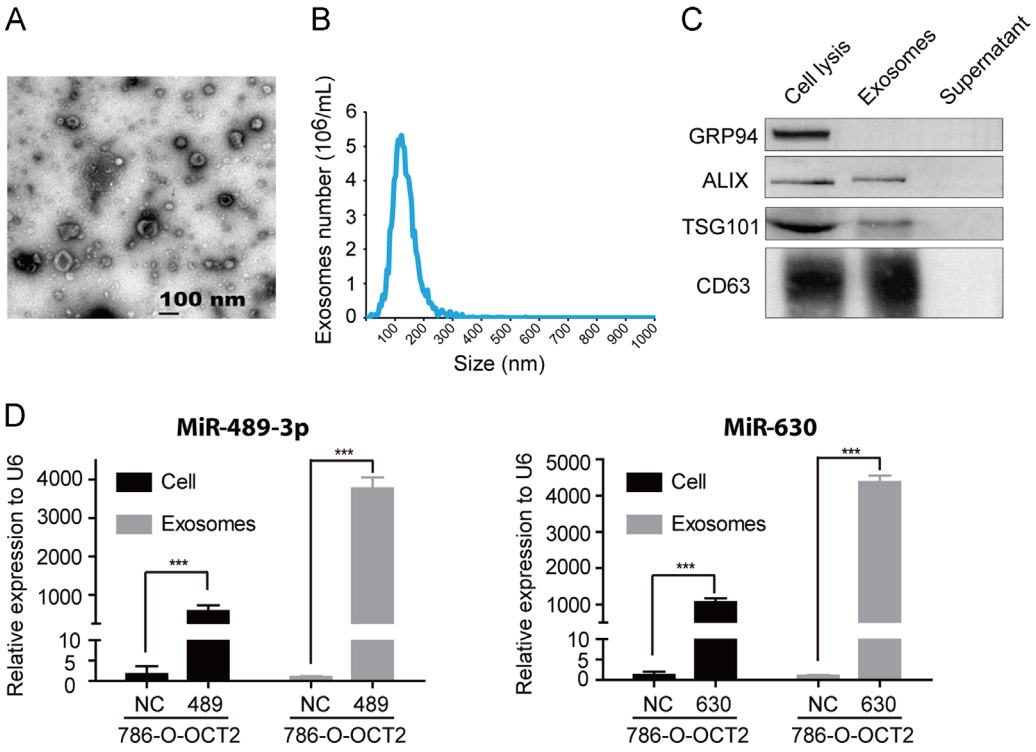

Figure 7 Potential of miR-489-3p and miR-630 as candidate biomarkers. (A) Representative electron microscopy images of exosomes secreted by 786-O-OCT2 cells. Scale bar, 100 nm. (B) ZetaView particle tracking analysis of the size distributions and number of exosomes. (C) Western blot analysis of protein markers in cells and exosomes. GRP94 (ab3674, Abcam) was rarely expressed in exosomes but rich in cells. ALIX (ab117600, Abcam), TSG101 (sc-7694, Santa Cruz) and CD63 (ab59479, Abcam) were all often used as identification protein marker of exosomes. (D) MiRNAs expression in 786-O-OCT2-NC, 786-O-OCT2-489 and 786-O-OCT2-630 cell lines and respective exosomes.

Unfortunately, the expression of these two miRNAs was not detected (data not shown) which may be due to the low stability of free miRNAs in the blood. The stability of exosomal miRNAs has enabled their feature as good biomarker candidates[28]. To the best of our knowledge, there is only one article presenting the possibility of exosomal miRNAs: miR-126-3p combined with miR-449a or with miR-34b-5p, extracted from urine as biomarkers of kidney cancer[8]. We isolated the exosomes derived from 786-O-OCT2-NC, 786-O-OCT2-489 and 786-O-OCT2-630 for miRNAs expression detection. Compared to the enrichment at the cell level, miR-489-3p and miR-630 were more abundant in exosomes isolated from miRNAs overexpression cell lines, which indicated that ccRCC cells may secrete massive dysregulated miRNAs by exosomes (Fig. 7D). The presence of miR-489-3p in exosomes, isolated from the urine of a ccRCC case and a normal case (Supporting Information Fig. S5) also suggested the potential of miR-489-3p as an auxiliary biomarker for early diagnosis of ccRCC. However, it still needs more clinical samples for verification. As deregulated miR-489-3p and miR-630 expression is an early event in tumorigenesis, measuring circulating miR-489-3p or miR-630 levels may also be valuable for early ccRCC detection, which can significantly contribute to the success of treatment.

Previously, the dysregulation of miR-630 has been widely identified in various cancers, including gastric cancer[29], hepatocellular carcinoma (HCC)[30], ovarian carcinoma[31], pancreatic cancer[32] and renal cell carcinoma[22], associated with cancer invasion, metastasis[29,33] and cell apoptosis[31]. In contrast to the upregulation in RCC, miR-489 was shown to be significantly reduced in human bladder cancer[34], colorectal cancer[35], breast cancer[36] and osteosarcoma[37], acting as a tumor-suppressive miRNA. However, only a few studies have figured out the regulation role that miR-630 and miR-489 play in cancer and the mechanisms leading to the upregulation of both in RCC have not yet been identified. Here, we elucidated part of the interaction between c-Myc and the promoter region of miR-630 that regulates miR-630 expression. However, some issues remain unclear: the possibility of other transcription factors involved in miRNAs regulation; the aberrantly expressed lncRNAs or circular RNAs may regulate the expression of miRNAs or OCT2, acting as competing endogenous RNAs (ceRNAs); the potential chromatin modifiers function at the promoter of miRNA; and other regulations on tumor growth and metastasis related proteins in RCC.

In addition to c-Myc, there is a binding site of P300, a key histone acetyltransferase, around 900 bp upstream of miR-630 TSS (Fig. S4), which implies that epigenetic regulation of histone acetylation may account for the increase of miR-630. The RCC cell lines 786-O, 769-P, CAKI and ACHN were treated with histone deacetylase inhibitor Vorinostat (SAHA) to enhance acetylation and qPCR results displayed upregulation of pri-miR-630 (Fig. S5). The results supported evidence of histone acetylation-dependent impact on miR-630, but this requires further investigation.

Hypoxia is a key pathological feature of solid tumors. Stabilized activation of hypoxia inducible factors (HIFs), a main tool for cells to cope with the stress, regulates the expression of various genes[38,39]. Studies have indicated that miR-630 is upregulated under hypoxic conditions in ovarian cancer[33]. MiR-489 is thought to be induced *via* hypoxia-inducible factor-1 during ischemic AKI to protect the kidneys in mice[40]. Quantification of precursors miR-489 and

miR-630 showed increased expression of pri-miR-489, pre-miR-489, pri-miR-630, and pre-miR-630 under hypoxic conditions, suggesting that miR-489 and miR-630 are transcriptionally upregulated (Fig. S5). However, the upregulation of mature miR-489-3p and miR-630 under hypoxia is not obvious, and may be due to other, as yet unknown, dysregulated factors in miRNA biosynthesis in RCC.

In cell-derived xenograft animal models, considering that stable-overexpression of genes will be lost during tumorigenesis, we detected the expression of *OCT2* and miRNA at the initial, middle and end stages of the experiment, confirming that overexpression of OCT2 and miRNAs were fully maintained. However, continuous passage cultivation makes cancer cell lines fit into an *in vitro* environment, which further leads to the loss of the tumor microenvironment. Recently, a patient-derived tumor xenograft (PDX) model has been successfully applied in research of RCC-target therapy[41,42] indicating PDX models are more convincible in elucidating the mechanisms of tumor progression and evaluating the efficacy of different cancer therapies. Our study is the first to show that overexpressed miR-489-3p and miR-630 repress OCT2 expression in RCC, resulting in oxaliplatin chemoresistance. Further studies on PDX models, treated with a combination of oxaliplatin and specific miRNA antagomir, will help further verify the correlation between OCT2 and miRNAs, and provide insight into clinical therapy of RCC.

5. Conclusions

In the current study, we reported a novel effect of miR-630 and miR-489-3p on OCT2, driving chemoresistance to oxaliplatin in RCC. We showed that the global upregulation in c-Myc is responsible for the transcriptional regulation of miR-630. Combinations of miRNA antagomirs in RCC therapy could sensitize cells to oxaliplatin and have important significance in guiding clinical chemotherapy.

Acknowledgments

This work was supported by grants from National Natural Science Foundation of China (81773817), The National Key Research and Development Program of China (2017YFC0908600), Fundamental Research Funds for the Central Universities (2017XZZX011-04, China) and Zhejiang University K.P.Chao's High Technology Development Foundation (China).

Appendix A. Supporting information

Supporting data associated with this article can be found in the online version at https://doi.org/10.1016/j.apsb.2019.01.002.

References

1. Bartel DP. MicroRNAs: target recognition and regulatory functions. *Cell* 2009;**136**:215–33.
2. Hanahan D, Weinberg RA. Hallmarks of cancer: the next generation. *Cell* 2011;**144**:646–74.
3. Cortez MA, Bueso-Ramos C, Ferdin J, Lopez-Berestein G, Sood AK, Calin GA. MicroRNAs in body fluids-the mix of hormones and biomarkers. *Nat Rev Clin Oncol* 2011;**8**:467–77.
4. Fabbri M. MiRNAs as molecular biomarkers of cancer. *Expert Rev Mol Diagn* 2010;**10**:435–44.
5. Sellitti DF, Doi SQ. MicroRNAs in renal cell carcinoma. *Microrna* 2015;**4**:26–35.
6. Jung M, Mollenkopf HJ, Grimm C, Wagner I, Albrecht M, Waller T, et al. MicroRNA profiling of clear cell renal cell cancer identifies a robust signature to define renal malignancy. *J Cell Mol Med* 2009;**13**:3918–28.
7. Lokeshwar SD, Talukder A, Yates TJ, Hennig MJP, Garcia-Roig M, Lahorewala SS, et al. Molecular characterization of renal cell carcinoma: a potential three-microrna prognostic signature. *Cancer Epidemiol Biomarkers Prev* 2018;**27**:464–72.
8. Butz H, Nofech-Mozes R, Ding Q, Khella HWZ, Szabo PM, Jewett M, et al. Exosomal microRNAs are diagnostic biomarkers and can mediate cell–cell communication in renal cell carcinoma. *Eur Urol Focus* 2016;**2**:210–8.
9. Lukamowicz-Rajska M, Mittmann C, Prummer M, Zhong Q, Bedke J, Hennenlotter J, et al. MiR-99b-5p expression and response to tyrosine kinase inhibitor treatment in clear cell renal cell carcinoma patients. *Oncotarget* 2016;**7**:78433–47.
10. Levi F, Ferlay J, Galeone C, Lucchini F, Negri E, Boyle P, et al. The changing pattern of kidney cancer incidence and mortality in Europe. *Bju Int* 2008;**101**:949–58.
11. Duran I, Lambea J, Maroto P, Gonzalez-Larriba JL, Flores L, Granados-Principal S, et al. Resistance to targeted therapies in renal cancer: the importance of changing the mechanism of action. *Target Oncol* 2017;**12**:19–35.
12. Singer EA, Gupta GN, Srinivasan R. Update on targeted therapies for clear cell renal cell carcinoma. *Curr Opin Oncol* 2011;**23**:283–9.
13. Heng DY, Xie W, Regan MM, Harshman LC, Bjarnason GA, Vaishampayan UN, et al. External validation and comparison with other models of the international metastatic renal-cell carcinoma database consortium prognostic model: a population-based study. *Lancet Oncol* 2013;**14**:141–8.
14. Zhu L, Wang J, Kong W, Huang J, Dong B, Huang Y, et al. LSD1 inhibition suppresses the growth of clear cell renal cell carcinoma *via* upregulating P21 signaling. *Acta Pharm Sin B* 2019;**9**:324–34.
15. Ding M, Lu X, Wang C, Zhao Q, Ge J, Xia Q, et al. The E2F1-miR-520/372/373-SPOP axis modulates progression of renal carcinoma. *Cancer Res* 2018.
16. Cho H, Du X, Rizzi JP, Liberzon E, Chakraborty AA, Gao W, et al. On-target efficacy of a HIF-2α antagonist in preclinical kidney cancer models. *Nature* 2016;**539**:107–11.
17. Yu Q, Liu Y, Zheng X, Zhu Q, Shen Z, Wang H, et al. Histone H3 lysine 4 trimethylation, lysine 27 trimethylation, and lysine 27 acetylation contribute to the transcriptional repression of solute carrier family 47 member 2 in renal cell carcinoma. *Drug Metab Dispos* 2017;**45**:109–17.
18. Liu YQ, Zheng XL, Yu QQ, Wang H, Tan FQ, Zhu QY, et al. Epigenetic activation of the drug transporter OCT2 sensitizes renal cell carcinoma to oxaliplatin. *Sci Transl Med* 2016;**8**.
19. An X, Sarmiento C, Tan T, Zhu H. Regulation of multidrug resistance by microRNAs in anti-cancer therapy. *Acta Pharm Sin B* 2017;**7**:38–51.
20. Wang K, Sun SY, Li LP, Tu MJ, Jiang HD. Involvement of organic cation transporter 2 inhibition in potential mechanisms of antidepressant action. *Prog Neuropsychopharmacol Biol Psychiatry* 2014;**53**:90–8.
21. Chow TFF, Youssef YM, Lianidou E, Romaschin AD, Honey RJ, Stewart R, et al. Differential expression profiling of microRNAs and their potential involvement in renal cell carcinoma pathogenesis. *Clin Biochem* 2010;**43**:150–8.
22. Zhao JJ, Chen PJ, Duan RQ, Li KJ, Wang YZ, Li Y. Up-regulation of miR-630 in clear cell renal cell carcinoma is associated with lower overall survival. *Int J Clin Exp Pathol* 2014;**7**:3318–23.
23. Garofalo M, Leva GD, Croce CM. MicroRNAs as anti-cancer therapy. *Curr Pharm Des* 2014;**20**:5328–35.
24. Niaz S. The AGO proteins: an overview. *Biol Chem* 2018;**399**:525–47.
25. Nilsson JA, Cleveland JL. Myc pathways provoking cell suicide and cancer. *Oncogene* 2003;**22**:9007–21.

26. Arsanious A, Bjarnason GA, Yousef GM. From bench to bedside: current and future applications of molecular profiling in renal cell carcinoma. *Mol Cancer* 2009;**8**:20.
27. Wang C, Hu JC, Lu ML, Gu HW, Zhou XJ, Chen X, et al. A panel of five serum miRNAs as a potential diagnostic tool for early-stage renal cell carcinoma. *Sci Rep* 2015;**5**.
28. Huang X, Liang M, Dittmar R, Wang L. Extracellular microRNAs in urologic malignancies: chances and challenges. *Int J Mol Sci* 2013;**14**:14785–99.
29. Chu DK, Zhao ZW, Li YM, Li JP, Zheng JY, Wang WZ, et al. Increased microRNA-630 expression in gastric cancer is associated with poor overall survival. *PLoS One* 2014;**9**:e90526.
30. Zhang JW, Li Y, Zeng XC, Zhang T, Fu BS, Yi HM, et al. miR-630 overexpression in hepatocellular carcinoma tissues is positively correlated with α-fetoprotein. *Med Sci Monit* 2015;**21**:667–73.
31. Eoh KJ, Lee SH, Kim HJ, Lee JY, Kim S, Kim SW, et al. MicroRNA-630 inhibitor sensitizes chemoresistant ovarian cancer to chemotherapy by enhancing apoptosis. *Biochem Biophys Res Commun* 2018;**497**:513–20.
32. Farhana L, Dawson MI, Murshed F, Das JK, Rishi AK, Fontana JA. Upregulation of miR-150* and miR-630 induces apoptosis in pancreatic cancer cells by targeting IGF-1R. *PLoS One* 2013;**8**:e61015.
33. Rupaimoole R, Ivan C, Yang D, Gharpure KM, Wu SY, Pecot CV, et al. Hypoxia-upregulated microRNA-630 targets Dicer, leading to increased tumor progression. *Oncogene* 2016;**35**:4312–20.
34. Li J, Qu WX, Jiang YZ, Sun Y, Cheng YY, Zou TJ, et al. MiR-489 suppresses proliferation and invasion of human bladder cancer cells. *Oncol Res* 2016;**24**:391–8.
35. Tao YM, Han T, Zhang T, Ma C, Sun CX. LncRNA CHRF-induced miR-489 loss promotes metastasis of colorectal cancer *via* TWIST1/EMT signaling pathway. *Oncotarget* 2017;**8**:36410–22.
36. Patel Y, Shah N, Lee JS, Markoutsa E, Jie CF, Liu S, et al. A novel double-negative feedback loop between miR-489 and the HER2-SHP2-MAPK signaling axis regulates breast cancer cell proliferation and tumor growth. *Oncotarget* 2016;**7**:18295–308.
37. Liu QF, Yang GC, Qian YY. Loss of microRNA-489-3p promotes osteosarcoma metastasis by activating PAX3-MET pathway. *Mol Carcinog* 2017;**56**:1312–21.
38. Majmundar AJ, Wong WJ, Simon MC. Hypoxia-inducible factors and the response to hypoxic stress. *Mol Cell* 2010;**40**:294–309.
39. Bertout JA, Patel SA, Simon MC. The impact of O-2 availability on human cancer. *Nat Rev Cancer* 2008;**8**:967–75.
40. Wei QQ, Liu Y, Liu PY, Hao JL, Liang MY, Mi QS, et al. MicroRNA-489 induction by hypoxia-inducible factor-1 protects against ischemic kidney injury. *J Am Soc Nephrol* 2016;**27**:2784–96.
41. Jimenez-Valerio G, Martinez-Lozano M, Bassani N, Vidal A, Ochoa-de-Olza M, Suarez C, et al. Resistance to antiangiogenic therapies by metabolic symbiosis in renal cell carcinoma PDX models and patients. *Cell Rep* 2016;**15**:1134–43.
42. Hong BA, Yang Y, Guo S, Duoerkun S, Deng XH, Chen DW, et al. Intra-tumour molecular heterogeneity of clear cell renal cell carcinoma reveals the diversity of the response to targeted therapies using patient-derived xenograft models. *Oncotarget* 2017;**8**:49839–50.
43. Su X, Wang H, Ge W, Yang M, Hou J, Chen T, et al. An *in vivo* method to identify microrna targets not predicted by computation algorithms: p21 targeting by miR-92a in cancer. *Cancer Res* 2015;**75**:2875–85.
44. Thery C, Amigorena S, Raposo G, Clayton A. Isolation and characterization of exosomes from cell culture supernatants and biological fluids. *Curr Protoc Cell Biol* 2006;**30**:3.22.1-29.